Equilibrium Polarization of Ultrathin $PbTiO_3$ with Surface Compensation Controlled by Oxygen Partial Pressure

M. J. Highland,[1,*] T. T. Fister,[2] D. D. Fong,[1] P. H. Fuoss,[1] Carol Thompson,[3] J. A. Eastman,[1] S. K. Streiffer,[4] and G. B. Stephenson[1]

[1]*Materials Science Division, Argonne National Laboratory, Argonne, Illinois 60439, USA*
[2]*Chemical Sciences and Engineering Division, Argonne National Laboratory, Argonne, Illinois 60439, USA*
[3]*Department of Physics, Northern Illinois University, DeKalb, Illinois 60115, USA*
[4]*Physical Sciences and Engineering Directorate, Argonne National Laboratory, Argonne, Illinois 60439, USA*

(Received 18 August 2011; published 25 October 2011)

We present a synchrotron x-ray study of the *equilibrium* polarization structure of ultrathin $PbTiO_3$ films on $SrRuO_3$ electrodes epitaxially grown on $SrTiO_3$ (001) substrates, as a function of temperature and the external oxygen partial pressure (pO_2) controlling their surface charge compensation. We find that the ferroelectric Curie temperature (T_C) varies with pO_2 and has a minimum at the intermediate pO_2, where the polarization below T_C changes sign. The experiments are in qualitative agreement with a model based on Landau theory that takes into account the interaction of the phase transition with the electrochemical equilibria for charged surface species. The paraelectric phase is stabilized at intermediate pO_2 when the concentrations of surface species are insufficient to compensate either polar orientation.

DOI: 10.1103/PhysRevLett.107.187602 PACS numbers: 77.80.bn, 64.70.Nd, 68.43.−h, 77.84.Cg

The presence of a phase transition between nonpolar and polar states in ferroelectric materials is responsible for their fascinating and useful properties such as divergent dielectric susceptibility, outstanding piezoelectric and pyroelectric coefficients, and the ability to switch between different stable polarization orientations through the momentary application of a field [1,2]. Recent studies have found that the extent of the compensation of the polarization by free charge at interfaces strongly affects the phase transition and thus the properties of ultrathin ferroelectric films and nanostructures [3–6]. Incomplete charge compensation due to finite electronic screening lengths in electrodes results in a residual depolarizing field and a reduction in the Curie temperature T_C [7–9]. Insufficiently compensated interfaces can result in the appearance of equilibrium 180° stripe domain and vortex polarization structures [5,6,10–13]. Competition between energy terms that scale with surface area and those that scale with volume results in large changes to the behavior as the system size decreases.

Charge compensation of ferroelectric surfaces without electrodes can involve extra or missing ions arising from interaction with the environment rather than electrons [14–21]. Sufficient ionic compensation can occur so that ultrathin films remain polar [15,16,22], and their polarization orientation can be controlled by changing the chemistry of the environment [17,20]. When the polarization orientation of $PbTiO_3$ films is inverted by changing the external oxygen partial pressure controlling ionic compensation, recent experiments [21] have found that, depending upon film thickness and temperature, the transition can occur either through the nucleation and growth of inverted domains or by a continuous mechanism, in which the polarization uniformly decreases to zero and inverts without the formation of domains. This crossover could be explained as an effect of either kinetics (e.g., limited nucleation rate) or thermodynamics (e.g., limited phase stability) in ultrathin films [21]. While first-principles theory [15,17–19] has confirmed that ionic compensation of surfaces is expected to be sufficient to stabilize polar phases in ultrathin ferroelectric films, the simple extrapolations used to apply these results to nonzero temperatures have not taken into account the ferroelectric phase transition. To date, most experiments on ultrathin ferroelectrics have been performed either in air [15,22–26] or in vacuum conditions [3,26–28], often without accounting for the possible large difference in equilibrium polarization stability. These considerations motivate the present work, the first determination of the *equilibrium* polarization phase diagrams of ultrathin ferroelectric films as a function of temperature and the external chemical potential controlling their ionic surface compensation.

Here we study epitaxial heterostructures consisting of ferroelectric $PbTiO_3$ (001) layers on conducting $SrRuO_3$ layers, both fully lattice-matched to $SrTiO_3$ single crystal substrates. This epitaxy constrains the $PbTiO_3$ polarization orientation in the film to be normal to the surface at the temperatures investigated [21,29]. The top surface of the $PbTiO_3$ is compensated by extra or missing oxygen ions produced by interaction with the environment—a controlled oxygen partial pressure (pO_2) in a flowing N_2 ambient at 13 mbar total pressure—while the bottom is compensated by electronic charge in the $SrRuO_3$. The films are grown by following procedures described elsewhere [15,17,21]. Grazing incidence x-ray scattering is used to characterize the atomic positions in the heterostructure.

X-ray measurements are performed *in situ* in the chamber used for $PbTiO_3$ film growth, at beam line 12ID-D of the Advanced Photon Source [17,21]. Values for the $PbTiO_3$ lattice parameter c and positive domain fraction x_{pos} are obtained by fitting the measured intensities along the $30L$ crystal truncation rod by using the calculated scattering from an atomic-scale model of the $PbTiO_3/SrRuO_3/SrTiO_3$ heterostructure as described previously [17,21]. The local polarization magnitude $|P|$ is obtained from c by using the well established relationship between strain and polarization in $PbTiO_3$ [29,30]. For each value of pO_2, data are obtained at successively lower temperatures by cooling from the nonpolar phase. In performing these experiments at constant pO_2, we find no significant dependence of the results upon whether a temperature is approached from above or below, in contrast to the large hysteresis observed when the film polarization orientation is switched by changing pO_2 at constant T [17,21]. Thus, a better determination of the equilibrium states is obtained by changing T at constant pO_2.

The measurements show that the temperature dependence of the $PbTiO_3$ polarization is a strong function of the external pO_2. Figure 1 shows $|P|$ versus T for a 5 nm $PbTiO_3$ film at three pO_2 values. The Curie temperature T_C below which the film polarizes is strongly suppressed at the intermediate pO_2 value. Values of c, x_{pos}, and $|P|$ as a function of T and pO_2 for 10-, 5-, and 3.5-nm-thick $PbTiO_3$ films are given in the Supplemental Materials [31]. These have been assembled to create the equilibrium phase diagrams shown in Fig. 2. Here the color scale represents the net polarization $\langle P \rangle \equiv |P|(2x_{pos} - 1)$, while the symbols show the phase observed at each point measured [31]. At lower T, the polarization has opposite sign for high and low pO_2 ($x_{pos} = 1$ and 0, respectively). The observed T_C (solid line) is minimum at the pO_2 value where the polarization orientation below T_C changes sign. The degree to which T_C is suppressed at these intermediate pO_2 values becomes greater as film thickness decreases. The square symbols show points where the crystal truncation rod fitting indicates a mixed domain structure with $0.13 < x_{pos} < 0.87$. At these points we typically observe diffuse scattering satellite peaks in the in-plane directions around the Bragg peak, indicating formation of equilibrium 180° stripe domains with periods in the range 12–25 nm [10,11].

The data presented in Figs. 1 and 2 are for a TiO_2 surface termination of the $PbTiO_3$, which we created at high temperature after growth by reducing the PbO vapor pressure in the chamber below the value that stabilizes the PbO surface termination [32]. We obtained a less extensive data set for the PbO surface termination, which we found to be more difficult to maintain consistently under all conditions for the length of time required for measurements

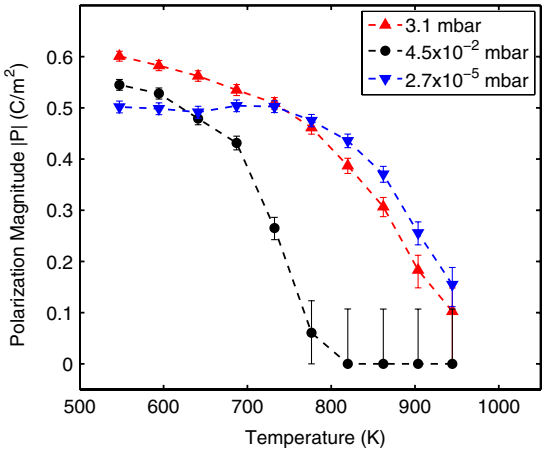

FIG. 1 (color online). Polarization magnitude vs temperature for a 5-nm-thick $PbTiO_3$ film on $SrRuO_3$ coherently strained to $SrTiO_3$ at three pO_2 values. The temperature below which the film polarizes (T_C) is significantly lower at the intermediate pO_2.

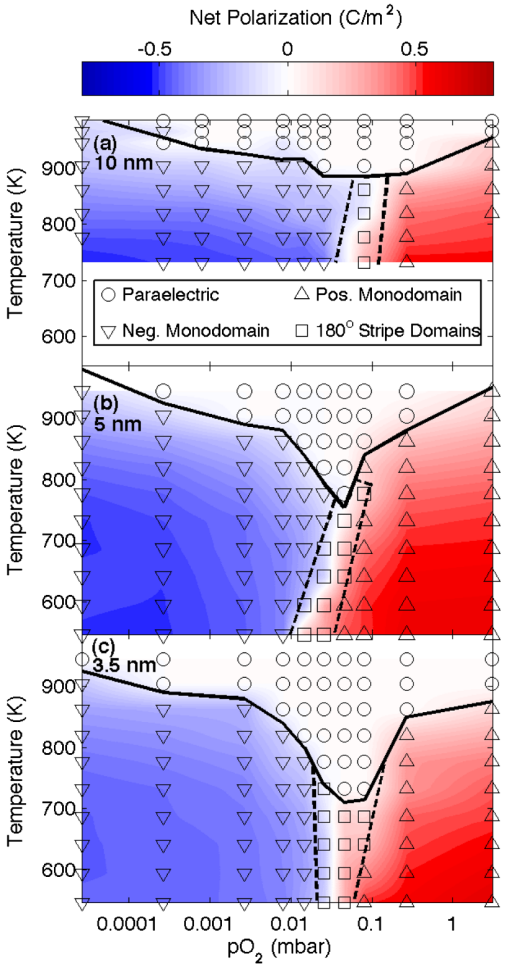

FIG. 2 (color online). Temperature vs pO_2 phase diagrams for three thicknesses of $PbTiO_3$ on $SrRuO_3$ coherently strained to $SrTiO_3$ (001). Color scale indicates net polarization. Symbols show points measured and phase observed. Solid lines indicate T_C, and dashed lines are boundaries of 180° stripe domain regions.

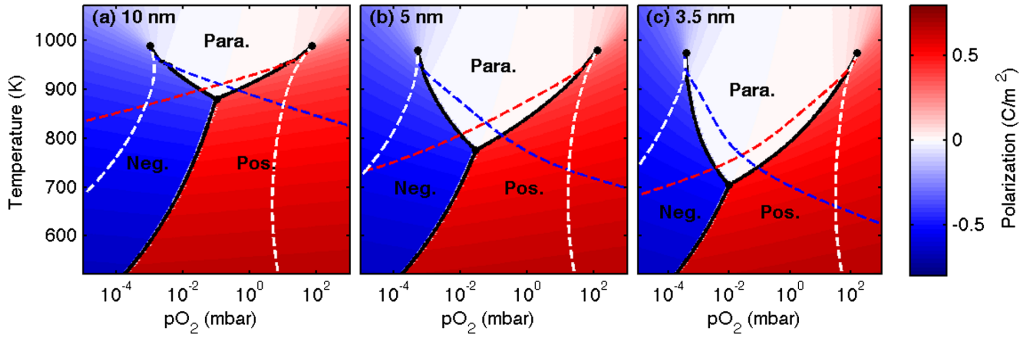

FIG. 3 (color online). Predicted polarization phase diagrams as a function of temperature and pO_2 for three thicknesses of $PbTiO_3$ on $SrRuO_3$ coherently strained to $SrTiO_3$ (001), from theory for ferroelectric films with ionic compensation [30]. Solid curves show equilibrium phase boundaries, and dashed red, blue, and white curves show metastability limits for the positive, negative, and paraelectric phases, respectively.

(e.g., 1 h per condition). The phase diagrams for both terminations are quite similar, with a minimum T_C at the pO_2 of the transition between positive and negative polar phases. For the 5 nm film, the PbO-terminated surface has a minimum T_C that is approximately 8 K lower and occurs a factor of 1.4 lower in pO_2 than the TiO_2-terminated surface.

While previous work [17,21] showed that the polarization orientation in ultrathin films could be inverted by changing between high and low pO_2, the equilibrium results in Figs. 1 and 2 show that applied oxygen potential is not equivalent to applied electric potential. Because $PbTiO_3$ coherently strained to $SrTiO_3$ has a second-order transition at zero field [29], if it were cooled under a nonzero applied electric field, the polarization would be expected to increase continuously without crossing a phase boundary between nonpolar and polar states [30]. Here we see a clear phase transition when cooling at each pO_2, with a T_C that varies with pO_2.

The experimental results can be qualitatively understood by considering the equilibrium concentrations of extra or missing surface ions and their interaction with the film polarization. Calculations using a model [30] based on Landau-Ginzburg-Devonshire theory for the ferroelectric phase transition supplemented by electrochemical equilibria for charged surface species are shown in Fig. 3. The Gibbs free energy per unit area is written as [30]

$$\mathcal{G} = t\left[f(P) + \frac{(\sigma + P)^2}{2\epsilon_0}\right] + \frac{\lambda^\dagger \sigma^2}{\epsilon_0} + \sum_{i=\ominus,\oplus} \frac{kT}{A}\left[\frac{\theta_i \Delta G_i^{00}}{kT} - \frac{\theta_i \ln pO_2}{n_i} + \theta_i \ln\theta_i + (1-\theta_i)\ln(1-\theta_i)\right], \quad (1)$$

where t is the ferroelectric film thickness, P is the polarization (assumed normal to the film surface), $f(P)$ is the standard Landau expansion of the free energy, σ is the compensating surface charge density, $\lambda^\dagger$ is the effective compensation screening length, A is the surface area per ion site, θ_i is the surface concentration of negative or positive species $i = \ominus$ or $\oplus$, respectively, and ΔG_i^{00} is their standard free energy of formation from n_i^{-1} O_2 molecules. The surface charge is related to the ion concentrations by $\sigma = \sum_i z_i e \theta_i / A$, where $z_i e$ is the ionic charge. Minimization of this free energy with respect to P and the θ_i yields the equilibrium polarization phase diagrams shown in Fig. 3, using the parameters in Table I. The values of n_i and z_i are consistent with doubly charged oxygen anions and vacancies as the negative and positive surface species, respectively, which have been found to stabilize monodomain polarization in *ab initio* calculations [15,17]. Note that the effective screening length $\lambda^\dagger$ can be negative in this model [30], because it includes a term from the polarization dependence of the ion formation energies.

The model qualitatively reproduces the observed minimum in T_C at an intermediate pO_2 value (where a triple point occurs between positive polar, negative polar, and paraelectric phases), as well as the increasing depth of this minimum as the film thickness becomes smaller. This stabilization of the paraelectric phase occurs because, at these pO_2 values, the surface ionic charge density is too low to compensate either polar state. The model also predicts a tilting of the positive or negative phase boundary below T_C towards lower pO_2 at lower T, for which there is some evidence in the experimental data. The model assumes that the film polarization is uniform and so does not capture the equilibrium 180° stripe domains that are observed along this boundary. While the terms in the sum in Eq. (1) used in the model produce transitions between the paraelectric and polar phases that are first order [30], the lack of a discontinuity in the measured $P(T)$ curves indicates that they may actually be second order. Alternatively,

TABLE I. Values of coefficients used in Fig. 3.

$\Delta G_\oplus^{00}$	0.87	(eV)	$\Delta G_\ominus^{00}$	0.17	(eV)
$n_\oplus$	-2		$n_\ominus$	2	
$z_\oplus$	2		$z_\ominus$	-2	
A	3.2×10^{-19}	(m^2)	$\lambda^\dagger$	-1×10^{-12}	(m)

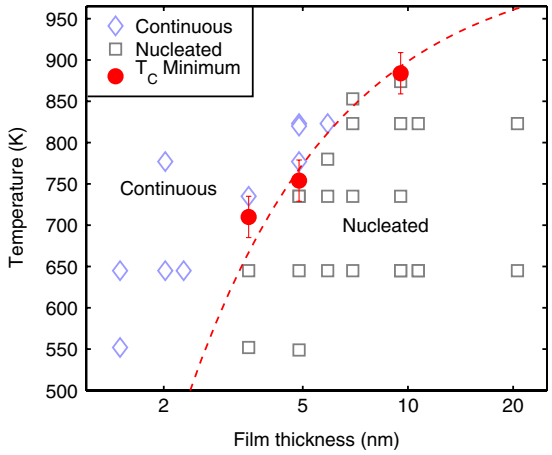

FIG. 4 (color online). Correspondence between regions of continuous and nucleated switching mechanisms found previously (open symbols) [21] and the minimum T_C observed in this work (solid circles). The dashed curve is a fit to $T_C^{\min} = T_C^0(1 - t^*/t)$, where $T_C^0 = 1023$ K is the zero-field T_C of $PbTiO_3$ coherently strained to $SrTiO_3$ [30] and $t^* = 1.2$ nm is the best fit value.

this may be an averaging of T_C due to inevitable nonuniformity of the film thickness on the single-unit-cell (0.4 nm) scale.

These results provide an explanation for the recent observation [21] of polarization switching without domain formation at the intrinsic coercive field in sufficiently thin $PbTiO_3$ films. Figure 4 shows the observed film thickness and temperature diagram [21] giving the regions for which polarization switching by changing pO_2 at constant temperature occurs by nucleation of oppositely polarized domains or, alternatively, by a continuous mechanism in which the local polarization magnitude passes through zero. Superimposed upon this diagram are three points corresponding to the minimum T_C from Fig. 2 for the three film thicknesses studied here. They correspond well with the boundary between the continuous and nucleated mechanisms of switching. This agreement implies that the change in the switching mechanism occurs because of equilibrium behavior rather than simply kinetic effects—the continuous mechanism occurs when, at the pO_2 where the parent polar phase loses stability, the stable phase is the nonpolar phase rather than the oppositely polarized or stripe phase. The instability curves shown on the calculated phase diagrams in Fig. 3 indicate that such regions can exist. If the transition is second order at T_C, then the instabilities would coincide with the phase boundaries. Furthermore, the internal field is predicted to reach the intrinsic coercive field at these instabilities. On the other hand, the regions of equilibrium 180° stripe domains on the phase diagrams of Fig. 2 indicate that the nucleated switching mechanism observed at these lower temperatures may occur through the initial formation of stripe domains.

These studies show that the chemical environment at the surface of an ultrathin ferroelectric film has strong effects on its phase transition. The nonpolar phase is stabilized and T_C is suppressed at intermediate chemical potentials where the concentrations of surface species are insufficient to compensate either orientation of the polar phase. Such ionic compensation offers a new tool for tuning ferroelectric properties and a new avenue for devices and must be considered when comparing studies carried out in different environments, e.g., ambient air or vacuum. While these results are for ionic compensation of surfaces, similar effects should occur at buried interfaces, such as that between a ferroelectric and an ionic conductor. Further development of the theory for ionic compensation and its validation through experiment will lay the ground work for fully understanding how a ferroelectric thin film interacts with its environment and for fully realizing the potential of ferroelectric materials.

This work was supported by the U.S. Department of Energy, Office of Science, Office of Basic Energy Sciences under Contract No. DE-AC02-06CH11357. The principle investigators and scientific program were supported by the Materials Sciences and Engineering Division, while use of the Advanced Photon Source was supported by the Scientific User Facilities Division.

*mhighland@anl.gov

[1] R. Ramesh and D. G. Schlom, MRS Bull. **33**, 1006 (2008).
[2] M. Dawber, K. M. Rabe, and J. F. Scott, Rev. Mod. Phys. **77**, 1083 (2005).
[3] M. F. Chisholm, W. Luo, M. P. Oxley, S. T. Pantelides, and H. N. Lee, Phys. Rev. Lett. **105**, 197602 (2010).
[4] A. M. Kolpak *et al.*, Phys. Rev. Lett. **105**, 217601 (2010).
[5] P. Zubko, N. Stucki, C. Lichtensteiger, and J.-M. Triscone, Phys. Rev. Lett. **104**, 187601 (2010).
[6] M. G. Stachiotti and M. Sepliarsky, Phys. Rev. Lett. **106**, 137601 (2011).
[7] I. P. Batra, P. Wurfel, and B. D. Silverman, Phys. Rev. Lett. **30**, 384 (1973).
[8] N. Sai, A. M. Kolpak, and A. M. Rappe, Phys. Rev. B **72**, 020101(R) (2005).
[9] M. Stengel, D. Vanderbilt, and N. A. Spaldin, Nature Mater. **8**, 392 (2009).
[10] S. K. Streiffer *et al.*, Phys. Rev. Lett. **89**, 067601 (2002).
[11] D. D. Fong *et al.*, Science **304**, 1650 (2004).
[12] B.-K. Lai, I. Ponomareva, I. Kornev, L. Bellaiche, and G. Salamo, Appl. Phys. Lett. **91**, 152909 (2007).
[13] C. Thompson *et al.*, Appl. Phys. Lett. **93**, 182901 (2008).
[14] S. V. Kalinin and D. A. Bonnell, Nano Lett. **4**, 555 (2004).
[15] D. D. Fong *et al.*, Phys. Rev. Lett. **96**, 127601 (2006).
[16] R. Takahashi *et al.*, Appl. Phys. Lett. **92**, 112901 (2008).
[17] R. V. Wang *et al.*, Phys. Rev. Lett. **102**, 047601 (2009).
[18] J. Shin *et al.*, Nano Lett. **9**, 3720 (2009).
[19] N. C. Bristowe, M. Stengel, P. B. Littlewood, J. M. Pruneda, and E. Artacho, arXiv:1108.2208v1.

[20] Y. Kim, I. Vrejoiu, D. Hesse, and M. Alexe, Appl. Phys. Lett. **96**, 202902 (2010).
[21] M. J. Highland *et al.*, Phys. Rev. Lett. **105**, 167601 (2010).
[22] C. Lichtensteiger, J.-M. Triscone, J. Junquera, and P. Ghosez, Phys. Rev. Lett. **94**, 047603 (2005).
[23] C. Thompson, C. M. Foster, J. A. Eastman, and G. B. Stephenson, Appl. Phys. Lett. **71**, 3516 (1997).
[24] D. D. Fong *et al.*, Phys. Rev. B **71**, 144112 (2005).
[25] S. V. Kalinin *et al.*, Phys. Rev. Lett. **100**, 155703 (2008).
[26] P. Maksymovych *et al.*, Phys. Rev. Lett. **102**, 017601 (2009).
[27] M. J. Bedzyk *et al.*, Phys. Rev. B **61**, R7873 (2000).
[28] L. Despont *et al.*, Phys. Rev. B **73**, 094110 (2006).
[29] N. A. Pertsev, A. G. Zembilgotov, and A. K. Tagantsev, Phys. Rev. Lett. **80**, 1988 (1998).
[30] G. B. Stephenson and M. J. Highland, Phys. Rev. B **84**, 064107 (2011).
[31] See Supplemental Material at http://link.aps.org/supplemental/10.1103/PhysRevLett.107.187602 for tables of c and x_{pos} obtained from fits and derived values of $|P|$ and $\langle P \rangle$.
[32] A. Munkholm *et al.*, Phys. Rev. Lett. **88**, 016101 (2001).